Journal of Alloys and Compounds 489 (2010) 614–619

Contents lists available at ScienceDirect

Journal of Alloys and Compounds

journal homepage: www.elsevier.com/locate/jallcom

ZnO hierarchical structures synthesized via hydrothermal method and their photoluminescence properties

Peng Huang[a,b], Xin Zhang[a,b], Jumeng Wei[a,b], Boxue Feng[a,b,*]

[a] Key Laboratory Magnetism and Magnetic Material of Education Lanzhou University, Lanzhou 730000, China
[b] Department of Physics, Lanzhou University, Lanzhou 730000, China

ARTICLE INFO

Article history:
Received 23 August 2009
Received in revised form
18 September 2009
Accepted 22 September 2009
Available online 30 September 2009

Keywords:
Zinc oxide
Chemical synthesis
Photoluminescence

ABSTRACT

The controlled synthesis of ZnO hierarchical structures has been successfully realized in a large scale via a simple hydrothermal method. It was demonstrated that the morphology of the final products was simply tuned by adding different amounts of soluble salt. ZnO microparticles were prepared when no soluble salt was added, whereas microspheres and nanoflowers were selectively prepared in the presence of different amounts of NaF. ZnO nanosheets were obtained when adding appropriate amount of NaCl, Na_2SO_4, or K_2SO_4. ZnO nanobelts were obtained in the presence of appropriate amount of sodium citrate ($C_6H_5Na_3O_7$). The photoluminescence (PL) properties of those products were researched, and the origin of the PL was discussed.

1. Introduction

Synthesis of nanomaterial with different morphologies has always being a focus for chemists and material scientists. Moreover, further research on the physical and chemical properties of nanomaterial is as important as synthesis. However, the physical and chemical properties of nanomaterials are always unpredicted as they differ greatly from their bulk counterparts [1–4]. Therefore, the controlled synthesis of nanomaterial is of great attraction and importance.

As one of the mostly utilized, fluorescent n-type semiconductor oxide, zinc oxide has wide bandgap energy (3.37 eV) and a large exciton binding energy (60 meV). It has been widely used as gas sensors [5], antireflective coating [6], photocatalyst [7], field-emission device [8], and in solar cells [9–11] due to its favourable structural, optical and catalytic properties.

Therefore, we are interested in developing simple method for morphology controlled fabrication of ZnO hierarchical structures. For a long period of time, morphology controlled fabrication of nanomaterials was usually achieved by two ways: (i) adding surfactant [12] and (ii) adjusting the pH values by acid or alkali [13–14]. Since sulfates influenced fabrication of tungsten oxide nanocrystals with different morphologies were reported, soluble salts were testified to play important roles in the synthesis of nanomaterials in solution environment. Morphology controlled or well dispersed nanomaterials were obtained by adding optimum amount of soluble salt [15,16]. Compared with above two conventional methods that adopted for morphology controlled fabrication, soluble salt affected fabrication has the advantage of low cost, facility, convenience, and diversification. In this paper, we report a simple hydrothermal method to synthesize ZnO crystals using zinc nitrate and hexamethylenetetramine as reaction material. Soluble salt such as Na_2SO_4, K_2SO_4, NaCl, KCl, NaF, and $C_6H_5Na_3O_7$ was used to tune the morphology of ZnO. Furthermore, the photoluminescence properties of ZnO hierarchical structures were characterized.

2. Experimental

All the chemicals were analytical grade. In a typical process, 2.5 mmol $Zn(NO_3)_2{\cdot}6H_2O$ and 2.5 mmol hexamethylenetetramine ($C_6H_{12}N_4$) were dissolved in 30 ml distilled water. After stirring for 20 min, the obtained homogeneous solution was transferred into a 50-ml teflonlined autoclave, distilled water was subsequently added up to 80% of its capacity. The autoclave was at last sealed and placed in an oven, heated at 90 °C for 24 h. Then the autoclave was cooled in air. The precipitate was centrifuged with deionized water and ethanol for 4 times at 6000 rpm for 5 min, respectively. Finally the resulting products were dried in an oven at 60 °C for 24 h.

The structure of the products was characterized by X-ray powder diffraction (Rigaku RINT2400 with Cu Kα radiation) and Micro-Raman spectrometer (Jobin Yvon LabRAM HR800 UV, YGA 532 nm). Field-emission scanning electron microscopy (FE-SEM S-4800, Hitachi) was employed for the morphology characterization. The photoluminescence properties of the products were characterized on Micro-Raman spectrometer (Jobin Yvon LabRAM HR800 UV, He-Cd 325 nm).

3. Results and discussion

The typical X-ray diffraction pattern of sample a was shown in Fig. 1. Sample a was obtained using 2.5 mmol $Zn(NO_3)_2{\cdot}6H_2O$ and

* Corresponding author at: Department of Physics, Lanzhou University, Lanzhou 730000, China. Fax: +86 931 8913554.
E-mail address: fengbx@lzu.edu.cn (B. Feng).

0925-8388/$ – see front matter.
doi:10.1016/j.jallcom.2009.09.127

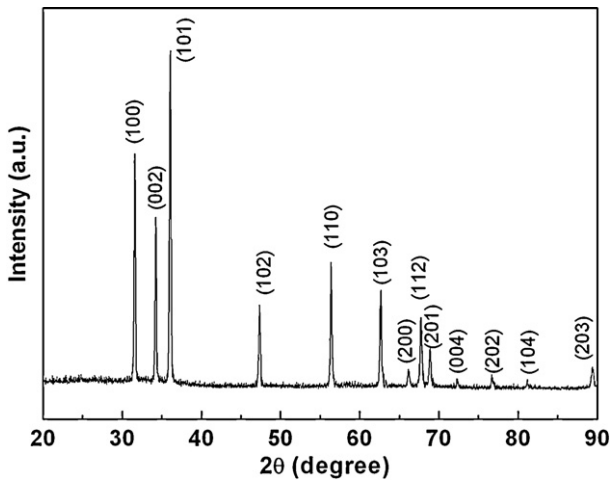

Fig. 1. XRD pattern of ZnO prepared without soluble salt.

Table 1
Reaction conditions of those products.

Samples	Soluble salt	Quantity of soluble salt (g)	Reaction temperature (°C)
a	/	/	90
b	NaF	0.5	90
c	NaF	1.0	90
d	$C_6H_5Na_3O_7$	0.5	90
e	$C_6H_5Na_3O_7$	1.0	90
f	NaCl	0.5	90
g	KCl	0.5	90
h	Na_2SO_4	0.5	90
i	K_2SO_4	0.5	90
j	NaF	0.5	120
k	NaF	1.0	120
1	$C_6H_5Na_3O_7$	0.5	120
m	$C_6H_5Na_3O_7$	1.0	120

2.5 mmol hexamethylenetetramine as reaction material (reaction system). All diffraction peaks can be indexed as the hexagonal phase of ZnO with the lattice constants $a = 0.325$ nm and $c = 0.5207$ nm, which is in good agreement with the JCPDS, No. 65-3411. Soluble salt such as NaF, $C_6H_5Na_3O_7$, NaCl, KCl, Na_2SO_4 and K_2SO_4 were used to tune the morphology of ZnO, whereas the reaction conditions were shown in Table 1.

Fig. 2(a) shows a low magnification SEM image of sample a at 90 °C. It can be found that the sample prepared without adding any soluble salt consists of a large quantity of microparticles. The mean diameter of those particles is about 10 μm. Some of them exhibit hexagonal prism like morphology. High magnification SEM image of sample a was shown in Fig. 2(b). It can be found that those particles are formed due to the accumulation of small-sized particles with mean size of about 2 μm.

The morphology of ZnO was significantly tuned in the presence of appropriate amount of soluble salt at 90 °C. When adding 0.5 g NaF to the reaction system, the morphology of ZnO changes to be sphere-like. It can be found from low magnification SEM image of sample b (Fig. 3(a)) that the mean diameter of those spheres is about 4 μm. Fig. 3(b) shows a high magnification SEM image of sample b. It can be found that those spheres are of coarse surfaces. It is proposed that the sphere like morphology comes from the etching effect of NaF [17]. It is not clear how does soluble salt affect the growth of crystal in solution environment, further investigations are under way in order to uncover the underlying principles of this observation. While tuning the amount of NaF, the morphology of the final products was as well tuned. Fig. 3(c) is a low magnification SEM image of sample c that prepared with 1.0 g NaF, which consists of flower-like ZnO with mean diameter of about 400 nm. A high magnification SEM image of sample c was shown in Fig. 3(d). It can be found that the flower-like ZnO nanostructures are composed of nanobelts. The mean width and length of those nanobelts are about 20 nm and 150 nm, respectively.

$C_6H_5Na_3O_7$ was also testified to be effective in tuning the morphology of ZnO. When 0.5 g $C_6H_5Na_3O_7$ was added to the system, the product turned to be belt-like. Low magnification SEM image of sample d was shown in Fig. 4(a), which indicates the sample makes up of a large quantity of nanobelts and a little amount of nanosheets. Fig. 4(b) is a high magnification SEM image of sample d that prepared with 0.5 g $C_6H_5Na_3O_7$. It can be found those nanobelts are about 5 μm in mean length, 60 nm in mean width, and tens of nanometer in thickness. The amount of $C_6H_5Na_3O_7$ has also played a key role in controlling the morphology of ZnO. Fig. 4(c) is a low magnification SEM image of sample e that prepared with 1.0 g $C_6H_5Na_3O_7$, which indicates coexistence of sheet-like and sphere-like morphology of ZnO crystals. It can be found from high magnification SEM image of sample e (Fig. 4(d)) that sphere-like morphology comes from the crispation of nanosheets.

Other soluble salts were also used to tune the morphology of ZnO crystals. Fig. 5 shows the SEM images of those samples obtained in the presence of different sorts of soluble salt at 90 °C. It can be found from Fig. 5(a) that sample f that prepared with 0.5 g NaCl consists of a large quantity of nanosheets with mean thickness of about 50 nm, and the diameter of those nanosheets ranges from 1 to 6 μm. Fig. 5(b) is a SEM image of sample g that prepared with 0.5 g KCl. The morphology of sample g turned to be microrod-based flower-like. The microrods are about 1 μm in mean diameter and 3 μm in mean length. A SEM image of sample h that prepared with 0.5 g Na_2SO_4 was shown in Fig. 5(c), which indicates that the mean diameter of those nanosheets is about 5 μm, and the thickness of those nanosheets is about 100 nm. Fig. 5(d) shows a SEM image of sample i that prepared with 0.5 g K_2SO_4, which was composed of

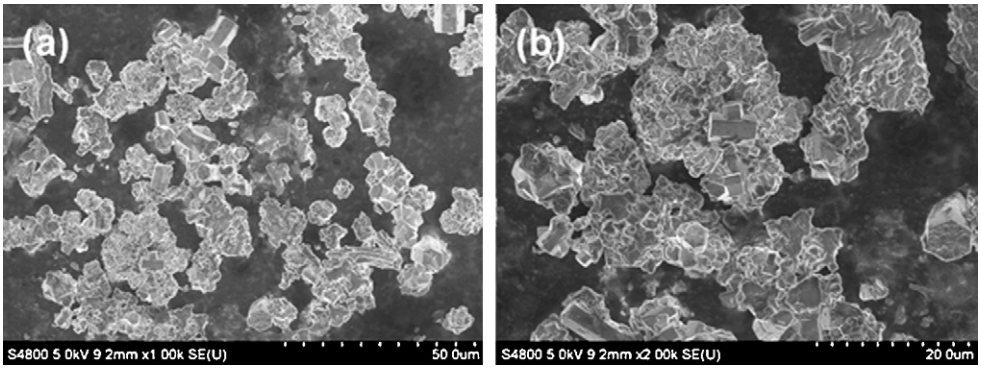

Fig. 2. SEM images of ZnO prepared without soluble salt with low (a) and high (b) magnification.

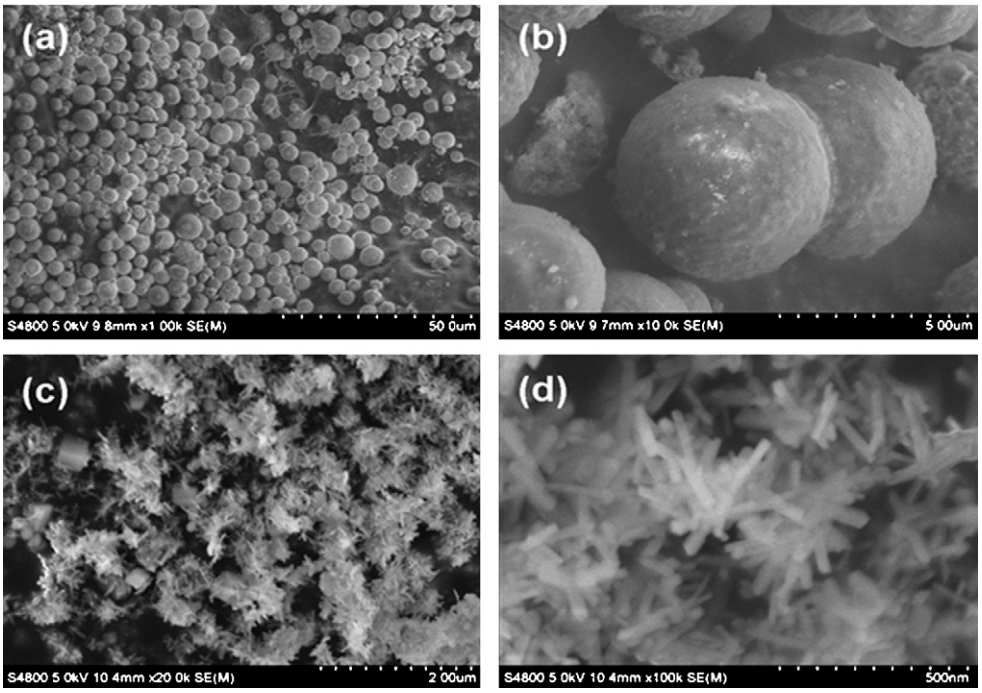

Fig. 3. Low (a) and high (b) magnification SEM images of ZnO prepared in the presence of 0.5 g NaF at 90 °C. Low (c) and high (d) magnification SEM images of ZnO prepared in the presence of 1.0 g NaF at 90 °C.

nanosheets with mean diameter about 20 μm and mean thickness about 100 nm. The morphology of samples f, g, and i does not significantly changed, but the size of those samples is much different. It indicates soluble salts have important effect on the growth of ZnO in solution environment. Both anions and cations play important roles in the growth of ZnO crystals. When tuning the amount of additive soluble salts (NaCl, KCl, Na_2SO_4, and K_2SO_4) or changing the reaction temperature, the morphology of the final products was not significantly changed.

It is well known that temperature plays an important role in the formation of crystal in hydrothermal process. The influence of temperature on the morphology of ZnO was also researched. It was found that the morphology of ZnO crystals was not distinctly affected by temperature in the presence of NaCl, KCl, Na_2SO_4, and

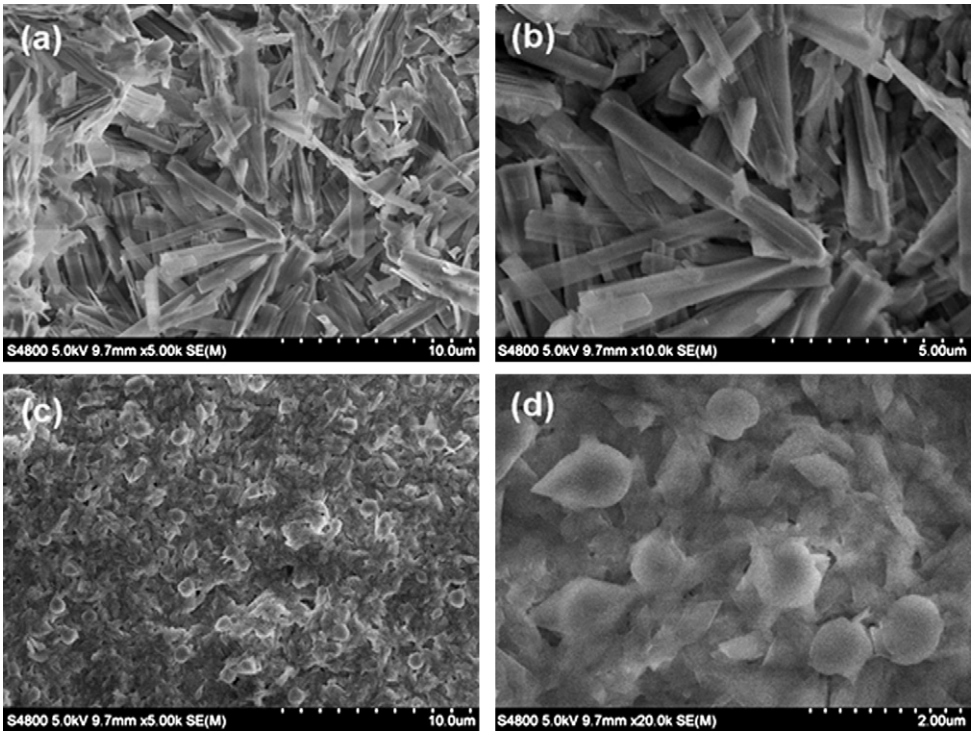

Fig. 4. Low (a) and high (b) magnification SEM images of ZnO prepared in the presence of 0.5 g $C_6H_5Na_3O_7$ at 90 °C. Low (c) and high (d) magnification SEM images of ZnO prepared in the presence of 1.0 g $C_6H_5Na_3O_7$ at 90 °C.

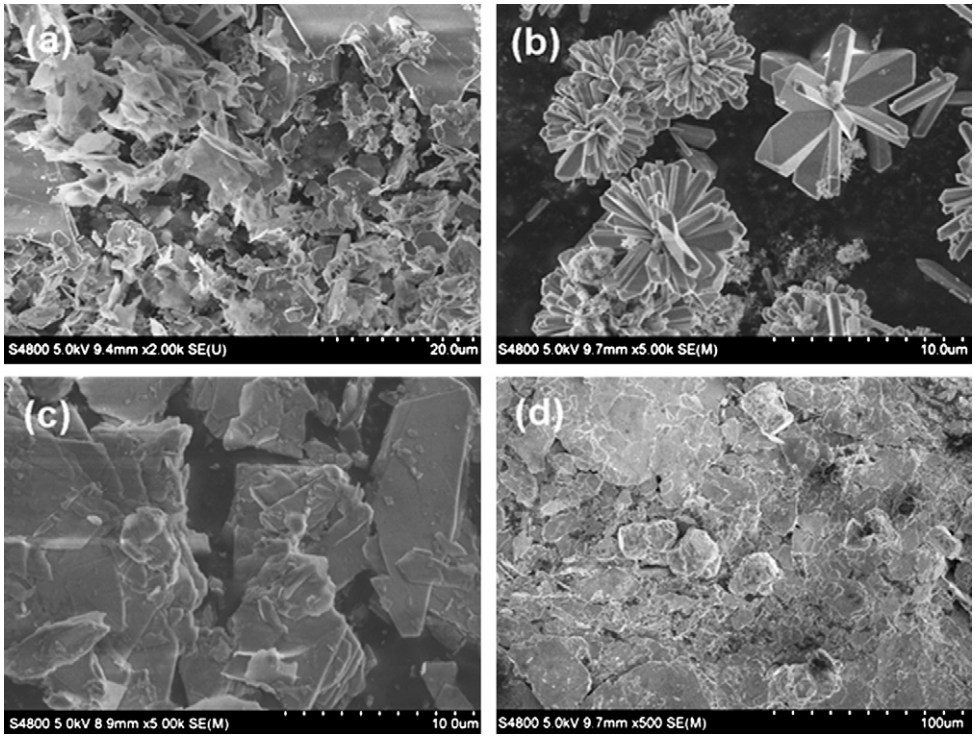

Fig. 5. SEM images of ZnO prepared in the presence of 0.5 g NaCl (a), 0.5 g KCl (b), 0.5 g Na_2SO_4 (c), and 0.5 g K_2SO_4 (d) at 90 °C.

K_2SO_4. However, the morphology of ZnO crystals was significantly affected by temperature in the presence of NaF and $C_6H_5Na_3O_7$. It can be found from Fig. 6(a) that sample j that prepared with 0.5 g NaF at 120 °C makes up of a large quantity of flower-like architectures with mean diameter of about 400 nm. The flower-like architectures are based on the accumulation of nanorods. The mean diameter and length of the nanorods is about 20 nm and 200 nm, respectively. Fig. 6(b) is a SEM image of sample k that prepared with 1.0 g NaF at 120 °C, which indicates the mean diameter of those urchin-like structures is about 5 μm. The urchin-like structures are composed of microrods, and the mean diameter and length of those microrods are about 300 mm and 2.5 μm, respectively. It can be found from Fig. 6(c) and (d) that sample l that prepared with 0.5 g $C_6H_5Na_3O_7$ at 120 °C and sample m that pre-

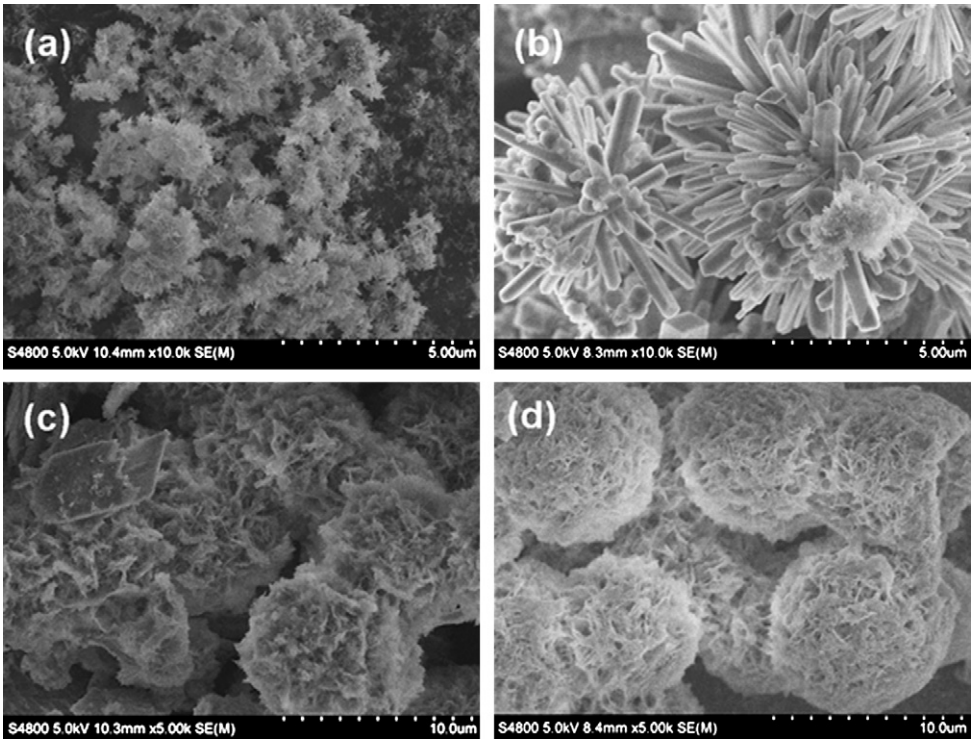

Fig. 6. SEM images of ZnO prepared in the presence of 0.5 g NaF (a), 1.0 g NaF (b), 0.5 g $C_6H_5Na_3O_7$ (c), and 1.0 g $C_6H_5Na_3O_7$ (d) at 120 °C.

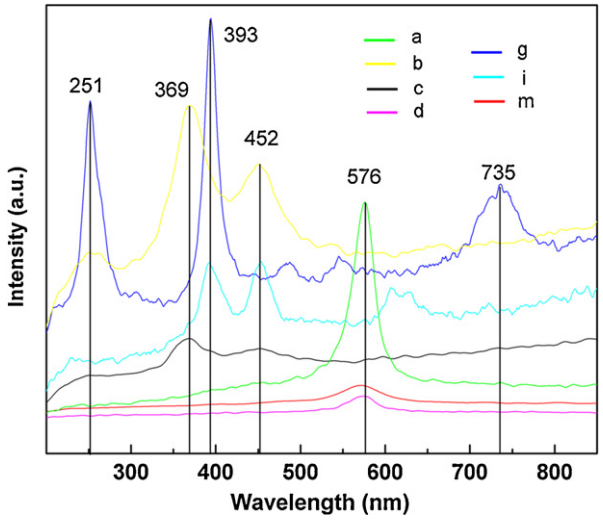

Fig. 7. Raman spectrum of ZnO hierarchical structures.

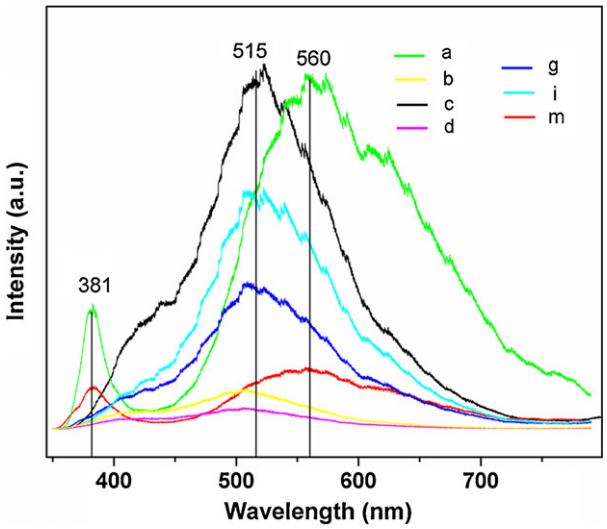

Fig. 8. Photoluminescence spectrum of ZnO hierarchical structures.

pared with 1.0 g $C_6H_5Na_3O_7$ at 120 °C are of flower-like structure with diameter of about 8 μm. The flower-like structures come from the accumulation of nanosheets. The nanosheets become to accumulate in the presence of 0.5 g $C_6H_5Na_3O_7$, and the accumulation is well developed when the amount of $C_6H_5Na_3O_7$ arrived at 1 g.

On the basis of the above experiment, it is obvious that the soluble salts play a key role in controlling the morphology of final products. Currently, the shape-controlled assembly mechanism is still unclear. However, it is believed that the inherent growth habit of the crystals as well as the specific interaction between the soluble salts and the crystal surfaces may have played an important role in controlling the morphology of the final crystals. Maybe, the different radius of Cl^-, SO_4^{2-}, F^- and $C_5H_7O_5COO^-$ anions and K^+ and Na^+ cations induce the different interactions between these anions and ZnO crystals, which leads to the different morphologies of the products [18].

Fig. 7 shows the Raman spectrum of ZnO hierarchical structures (sample a (particle), b (sphere), c (rod), d (belt), g (flower), I (sheet), and m (urchin-like)). The peaks are associated with those of ZnO. The peak at 369 cm^{-1} should be assigned to the A_{1T} mode, and the peak at 393 cm^{-1} should be assigned to E_{1T} mode [19]. The peak at 452 cm^{-1} corresponds to the E_2 mode of ZnO crystal, while the peak at 576 cm^{-1} corresponds to E_1 (LO) mode of oxygen deficiency [20–22]. Normally, the low-frequency Raman peaks are assigned to lattice vibrations. So the bands observed at 251 cm^{-1} may be caused due to the deformation mode [23]. The peak at 735 cm^{-1} may ascribe to the second-order photo modes $B_1 + LO$ [24]. The solution environment was affected by different sorts of soluble salt, leading to disparate growth of ZnO hierarchical structures. In addition, Raman peaks of ZnO that obtained in the presence of different sorts of soluble salt are much different, which indicate that the crystal growth of ZnO was affected by soluble salt. Further investigation on the soluble salt affected growth mechanism of ZnO should be done to clarify the difference of Raman spectrum.

Fig. 8 shows the photoluminescence emission spectra of ZnO hierarchical structures (samples a–d, g, i, and m) applying 325 nm excitation wavelength. Samples a and d show two emission peaks located at 381 nm and 560 nm, which are the typical near-band edge and defects related emissions of ZnO. We propose the green emissions located at 560 nm are attributed to oxygen vacancies, which could be seen from Raman peaks located at 576 cm^{-1}. The emission intensity decreases while adding appropriate amount of $C_6H_5Na_3O_7$, which may be related to the decrease of oxygen vacancies, and in accordance with the intensity of Raman peaks located at 576 cm^{-1}. It can be found that samples b, c, g, i, and m show one distinct emission peak located at near 515 nm, whereas the near-band edge emission peak is not so observable. The blue shift of the green emission may originate from different chemical surrounding of the oxygen vacancies [25], which was affected by different sorts of soluble salt. The intensity of green emission decreases due to the reduction of oxygen vacancies, which was in accordance with Raman peaks. It is further indicated that the inner crystal structure of ZnO was obviously affected by soluble salt. Different sorts of soluble salt have different effects on the growth of ZnO crystals, leading to the formation of ZnO hierarchical structures.

4. Conclusion

In conclusion, we have synthesized ZnO hierarchical structures in the presence of different sorts of soluble salt. Room temperature photoluminescence properties of the as-synthesized products were characterized using an excitation wavelength of 325 nm. The strong green emissions are attributed to the oxygen vacancies, shifting to low wavelength region in the presence of appropriate amount soluble salt. This soluble salt affected method may be widely adopted in hydrothermal synthesis due to its simpleness, facility, and low cost. As the origin of soluble salt affected synthesis is unclear by now, further work should be done to clarify it, which are relevant to the origin of the difference of the photoluminescence properties of ZnO hierarchical structures.

Acknowledgement

This work was funded by the National Sciences Foundation of China (grant No. 60536010 and 60576013).

References

[1] A.P. Alivisatos, Science 271 (1996) 933–937.
[2] V. Pachauri, C. Subramaniam, T. Pradeep, Chem. Phys. Lett. 423 (2006) 240–246.
[3] W. Merchan-Merchan, A.V. Saveliev, L.A. Kennedy, Chem. Phys. Lett. 42 (2006) 72–77.
[4] C. Burda, X. Chen, R. Narayanan, M.A. El-Sayed, Chem. Rev. 105 (2005) 1025–1102.
[5] R. Ferro, J.A. Rodríguez, P. Bertrand, Thin Solid Films 516 (2008) 2225–2230.
[6] Y.J. Lee, D.S. Ruby, D.W. Peters, B.B. Mckenzie, J.W.P. Hsu, Nano Lett. 8 (2008) 1501–1505.
[7] T. Szabó, J. Németh, I. Dékány, Colloids Surf. A: Physicochem. Eng. Aspects 230 (2004) 23–35.
[8] H.B. Zeng, X.J. Xu, Y. Bando, U.K. Gautam, T.Y. Zhai, X.S. Fang, B.D. Liu, D. Golberg, Adv. Funct. Mater 19 (2009) 3165–3172.

[9] M. Krunks, A. Katerski, T. Dedova, I.O. Acik, A. Mere, Solar Energy Mater. Solar Cells 92 (2008) 1016–1019.
[10] B. Asenjo, A.M. Chaparro, M.T. Gutierrez, J. Herrero, J. Klaer, Solar Energy Mater. Solar Cells 87 (2005) 647–656.
[11] A. Strohm, L. Eisenmann, R.K. Gebhardt, A. Harding, T. Schlözer, D. Abou-Ras, H.W. Schock, Thin Solid Films 480–481 (2005) 162–167.
[12] G.F. Zou, K. Xiong, C.L. Jiang, H. Li, T.W. Li, J. Du, et al., J. Phys. Chem. B 109 (2005) 18356–18360.
[13] X.L. Zhang, C.H. Sui, J. Gong, Z.M. Su, L.Y. Qu, J. Phys. Chem. C 111 (2007) 9049–9054.
[14] C. Jia, Y. Cheng, F. Bao, D.Q. Chen, Y.S. Wang, J. Crystal Growth 294 (2006) 353–357.
[15] Y. Sun, D.J. Riley, M.N.R. Ashfold, J. Phys. Chem. B 110 (2006) 15186–15192.
[16] R. Yi, H.F. Zhou, N. Zhang, G.Z. Qiu, X.H. Liu, J. Alloys Compd. 479 (2009) L50–L53.
[17] X. Wang, H.B. Fu, A.D. Peng, T.Y. Zhai, Y. Ma, F.L. Yuan, et al., Adv. Mater. 21 (2009) 1636–1640.
[18] Z.J. Gu, T.Y. Zhai, B.F. Gao, X.H. Sheng, Y.B. Wang, H.B. Fu, et al., J. Phys. Chem. B 110 (2006) 23829–23836.
[19] J.F. Xu, W. Ji, X.B. Wang, H. Shu, Z.X. Shen, S.H. Tang, J. Raman Spectrosc. 29 (1998) 613–615.
[20] X. Wang, Q. Li, Z. Liu, J. Zhang, Z. Liu, R. Wang, Appl. Phys. Lett. 84 (2004) 4941–4943.
[21] X.L. Xu, S.P. Lau, J.S. Chen, G.Y. Che, B.K. Tay, J. Cryst. Growth 223 (2001) 201–205.
[22] J.J. Wu, S.C. Liu, J. Phys. Chem. B 106 (2002) 9546–9551.
[23] D. Behera, B.S. Acharya, J. Lumin. 128 (2008) 1577–1586.
[24] M.S. Jang, M.K. Ryu, M.H. Yoon, S.H. Lee, H.K. Kim, A. Onodera, et al., Curr. Appl. Phys. 9 (2009) 651–657.
[25] E. Pál, V. Hornok, A. Oszkó, I. Dékány, Colloids Surf. A: Physicochem. Eng. Aspects 340 (2009) 1–9.